

Received January 1, 2020, accepted February 9, 2020, date of publication February 12, 2020, date of current version February 20, 2020.

Digital Object Identifier 10.1109/ACCESS.2020.2973341

Development and Verification of Mechanism for Enhancement of Steering Angle and Active Locomotion for Magnetic Micro Active-Guidewire

GUK-HONG JEON¹ AND SUNG HOON KIM^{1,2}, (Member, IEEE)

¹New Technology Convergence Team, CAMTIC Advanced Mechatronics Technology Institute, Jeonju 54852, South Korea

²Department of Electronics Convergence Engineering, Wonkwang University, Iksan 54538, South Korea

Corresponding author: Sung Hoon Kim (kshoon@wku.ac.kr)

This work was supported by the Basic Science Research Program of the National Research Foundation of Korea (NRF) through the Ministry of Education and the Ministry of Science, ICT and Future Planning under Grant NRF-2015R1D1A1A01057463 and Grant 2018R1C1B6003491.


ABSTRACT In this study, the authors developed a novel active guidewire including a spiral-type magnetic microrobot and ball joint to realize active locomotion and improve the steering capability within external magnetic fields. Most active guidewires provide only steering ability without active locomotion, and their steering angles depend on the physical properties of the wire. The developed mechanism provides a wider range of steering angles because the total steering angle is the sum of the joint angle and wire angle. To evaluate the performance of the proposed mechanism, we compared and analyzed the steering and active locomotion in a dc field and rotating magnetic field in conditions involving and not involving the ball joint mechanisms. At a low magnetic field strength (up to 4 kA/m), considerable improvement in the steering angle owing to the use of the ball joint was noted. The dc and rotating fields with an intensity of 8 kA/m generated peak steering angles of 189° and 135°, respectively. Various experiments were conducted, and the results confirmed that the proposed mechanism could improve the steering ability while realizing active locomotion. In particular, the steering stability and movement ability corresponding to different types of magnetic fields could be analyzed.

INDEX TERMS Active guidewire, ball joint, spiral-type magnetic microrobot, steering ability, electromagnetic field control.

I. INTRODUCTION

Magnetically actuated microrobots have been developed for biomedical applications [1]–[5]; In particular, owing to their small size and ability to be wirelessly controlled without the need for implanted batteries, magnetic microrobots can be applied to minimally invasive treatments to enable diagnosis and therapy in medicine, such as for sensing, targeted drug delivery, hyperthermia, active guidewire applications, and performance of biopsy [6]–[11]. For active locomotion of magnetic microrobots, a certain magnetic force and magnetic torque are required according to the associated robot mechanism. The control of magnetic force and magnetic torque can lead to the generation of translational and rotational movement, respectively, to enable active locomotion. The mobility and steerability of magnetic microrobots are

desirable factors that can enable their potential application in active guidewires or catheter systems. Conventional catheterization requires reasonable control skill because medical doctors must control the tip of the guidewire via motion that is induced from outside the patient's body. In such a case, the condition of the tip of the guidewire is also critical for steering; If the tip is twisted, it is difficult to steer the guidewire. To avoid these issues, active guidewires have been developed, in which controllable steering is realized using a multi-joint mechanism based on shape memory alloy (SMA) or shape memory polymer actuators (SMP), and magnetic actuation is realized using magnetic torque and force [12]–[16]. Typically, the steering of magnetically actuated guidewires is driven by the magnetic force or magnetic torque. In general, an applied magnetic field gradient generates translational motion via the magnetic force, whereas a uniform magnetic field can produce rotation via the magnetic torque to enable the control of magnetic microrobots [17]–[23]. The rotating

The associate editor coordinating the review of this manuscript and approving it for publication was Yizhang Jiang .

motion corresponds to better mobility and steerability than translational movement does.

Magnetically actuated guidewires can be structurally simple and easy to control in comparison to guidewires using SMA, SMP, and other smart materials. In particular, these guidewires can be miniaturized owing to the realization of wireless control. Therefore, several research groups have attempted to develop magnetically actuated active guidewires. Krings *et al.*, [24] used two permanent magnets for position control of a 0.0014-inch magnetic microguidewire; the tip in this case was a permanent magnet of 2 mm, and the system produce a high-intensity magnetic field of 0.1 T. Clogenson *et al.*, introduced steerable guidewire that was compatible with the MRI environment and thus could be applied for endovascular interventions [25]. Jeon *et al.*, realized precise steering and unclogging motions of a catheter, which consisted of a flexible tube and permanent magnet (15.7 mm³ in volume) [26]. Choi *et al.*, introduced a magnetically actuated flexible microrobot (with a magnet diameter and length of 0.4 mm and 0.8 mm, respectively) to improve the steerability of a guidewire. The guidewire was driven by a 15mT field, and generated a steering angle of up to 80° in a dc magnetic field [27]. Jeon *et al.* developed a magnetically controlled soft microrobot using two permanent magnets with PDMS for steering a guidewire [28]. The robot contains two separate magnets, which have a diameter and length of 0.4 and 0.8 mm, respectively. Using the robot, maximum steering angle of 132.7° was achieved at 15 mT. Kim *et al.* developed a magnetic catheter with rotating multi-magnets for unclogging motions with enhanced steering capability [29]. The magnetic catheter contained two separate magnets: the outer diameter, inner diameter and length were 2, 1, and 5 mm, respectively. The magnetic catheter generated a steering angle of 60° at 14 mT. All these magnetic guidewires exhibited steerability, although they were unable to realize active locomotion. Therefore, their mobility was controlled by a feeding device or the hand control of medical doctors. To realize active locomotion with steering for a guidewire, we previously employed a spiral-type magnetic microrobot, and the proposed system could realize active locomotion with steering in a three-axis Helmholtz coil [16]. Although the system generated relatively small steering angles of less than 50° at 10 mT, the approach represented a valuable technique that could help realize steering with active locomotion. Using the screw mechanism, the robot could perform drilling in blood vessels to remove clots. The system was in contrast to most magnetic active guidewires that demonstrate low steering angles of less than 90° and cannot realize active locomotion. In order words, the guidewire is a very difficult or impossible to change the steering more than 90 degrees in a very narrow moving space. Therefore, a mechanism is needed to create a large steering angle at the end of the wire.

In this study, we proposed a new mechanism for enhancement of steerability and active mobility. The developed robotic guidewire has significant implication for minimally

invasive interventional medicine technology. In particular, the proposed mechanism and methods can realize a highly safe, high-precision automated multifunctional active micro-catheter system for diagnosis and therapy, such as treating an aneurysm associated with conventional active guidewire. The proposed method and its advantages are as follows:

- (1) We propose a ball joint mechanism that can innovatively adjust the steering angle.
 - Enhancement of maximum steering angle ($\theta_S = \theta_J + \theta_W$): wire angle (θ_W) and joint angle (θ_J).
 - Wider range of magnetic field strengths for steering, from 1 kA/m.
- (2) Spiral-type mechanism for 3D active locomotion and precision control using a rotating magnetic field and dc magnetic field.
- (3) Effective thrombus removal function by generating a rotating and tilting motion of the spiral-type microrobot using the ball joint mechanism.

A spiral-type magnetic microrobot was applied as the tip of a guidewire to enable active locomotion. The robot and the guidewire were connected by a ball-joint to improve the steering angle. In general, the steering angle of a guidewire depends on flexible property of the guidewire. Therefore, the steering angle corresponds to the bending angle of the wire. The steering angle of the proposed mechanism was divided into two angles: joint angle and wire bending angle. The developed ball-joint could produce a maximum joint angle of up to 45° without the wire bending. We compared the steering angles of the guidewire with the ball joint to those of a guidewire without the ball joint in a dc magnetic field and rotating magnetic field. The proposed mechanism produced a steering angle of approximately 90° at the extremely low magnetic field of 2 kA/m, and it generated steering angles of approximately 170° and 120° at the dc and rotating fields of 8 kA/m, respectively. The rotating magnetic field corresponded to a more stable steering ability than the dc magnetic field did because the robot and wire were aligned in the direction of the rotation axis. Through various experiments, we have improved the steering angle and verified the active movement using the proposed mechanism at a low magnetic field strength.

II. MECHANISM AND MANIPULATION OF THE PROPOSED SYSTEM

A. BALL JOINT-BASED END-EFFECTOR FOR ENHANCEMENT OF STEERING

We proposed a novel active guidewire mechanism that employs a ball joint mechanism with a spiral-type magnetic microrobot to improve the steering angle of active guidewire as well as active locomotion. Figure 1 shows the configuration of the proposed mechanism and the conditions for steering via the ball joint mechanism. The proposed active guidewire consists of a spiral-type magnetic microrobot, ball joint, and guidewire, as shown in Fig. 1 (a). The microrobot is synchronized via a rotating magnetic field. In particular,

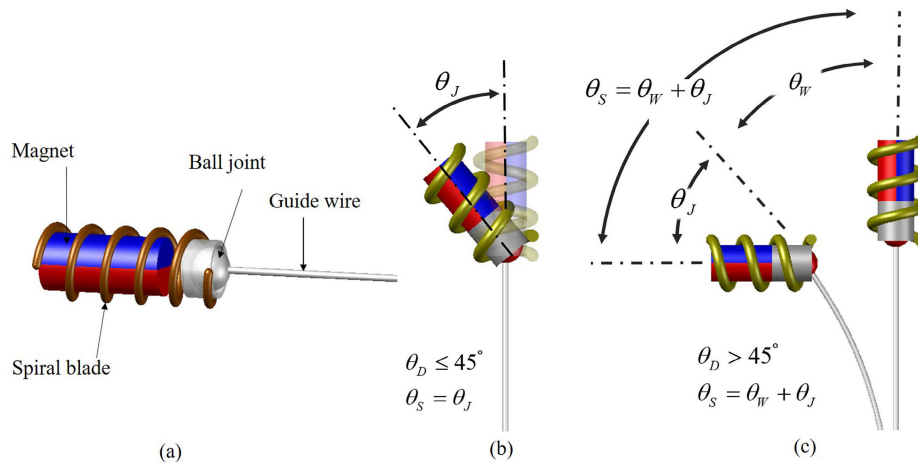


FIGURE 1. Mechanism for enhancement steering angle and active locomotion: (a) Configuration of the proposed mechanism, (b) Steering angle by a ball joint angle, and (c) principle of generation of the improved steering angle by the joint angle θ_J and the wire angle θ_W .

the ball joint connects the robot and the guidewire while the robot rotates to tow and steer the wire.

In general, the steering angle for magnetically actuated guidewires is the result of the deformation of a guidewire, and active locomotion is not employed. Therefore, the generated steering angles are small, with values of less than 90° . However, because the developed active guidewire utilizes the ball joint mechanism, two steering angles corresponding to the deformation and ball joint angles are generated. In this manner, the proposed mechanism can provide steering angles of up to 150° . In addition, the spiral-type magnetic microrobot provides two functions: the realization of active locomotion and drilling in blood vessel to remove clots. The fabricated ball joint can provide a joint angle of up to 45° along with no wire deformation, as shown in Fig. 1 (b). Therefore, when the desired angle θ_D is 45° or less, the steering angle θ_S is the joint angle θ_J . If the desired steering angle is more than 45° , the steering angle of the proposed guidewire is the sum of the joint angle and wire angle (θ_W), that is the total steering angle is $\theta_S = \theta_J + \theta_W$, as shown in Fig. 1 (c). The proposed ball joint mechanism not only provides a wide steering angle but also provides precise control and tilting of the position of the end effector in the rotating magnetic field. The tilt angle is equal to the ball-joint angle.

B. MAGNETIC MANIPULATION TO REALIZE STEERING AND ACTIVE LOCOMOTION

Because of the presence of the ball joint in the end-effector of the proposed mechanism, the developed guidewire provides a wider range of steering angle than can be generated using general guidewire. In particular, the end-effector of the spiral mechanism can help realize active locomotion.

Because the end-effector contains a magnet, steering is controlled via an external magnetic field. The direction and strength of the magnetic torque between a magnet and an applied magnetic field determine the steering direction and

angle. The magnetic torque can be expressed as follows:

$$\mathbf{T} = \mathbf{M} \times \mathbf{B}_{ext} \quad (1)$$

where \mathbf{M} is the magnetic moment and \mathbf{B}_{ext} is the external magnetic field density. Figure 2 shows the steering methods according to the type of magnetic field applied, in particular, dc or rotating magnetic fields. Method_1 represents the typical solution for steering using dc fields (uniform or gradient fields). In this case, the guidewire can generate steering without active locomotion, as shown in Fig. 2 (a). The magnetic torque between the applied field and the end-effector is aligned to the desired direction. However, Method_2, which uses a rotating magnetic field, leads to the realization of both steering and active locomotion, as shown in Fig. 2 (b). When a rotating magnetic field is applied, the end-effector is synchronized to the rotating magnetic field by the magnetic torque and generates propulsive force for active locomotion. In this case, the direction of movement of the guidewire changes according to the control of two angles, namely, α and ζ . The control of angle α can lead to longitudinal steering of the plane of the rotating magnetic field, and that of angle ζ can help realize lateral steering of this plane.

Therefore, three-dimensional movement and steering can be realized by controlling two angles. Figure 2 (c) shows the fabricated robotic guidewire. The microrobot includes a cylindrical NdFeB magnet with dimensions of $\text{Ø}1.8 \text{ mm} \times 3 \text{ mm}$ and moment of $7.1 \times 10^{-3} \text{ Am}^2$, along with spiral blades with a pitch of 1.5 mm and blade angle of 70° . The employed magnet has a radial direction of magnetization. The robot can be produced with a diameter of less than 1 mm, in which case, it can be applied to the cardiovascular guidewire.

Rotation of the end-effector generates thrust owing to the spiral mechanism, as shown in Fig. 2 (c). The generated thrust of the end-effector can be expressed as follows [6]:

$$\mathbf{F}_t = \mathbf{F}_n \cos \beta_n \cos \delta - \mathbf{F}_f \sin \delta \quad (2)$$

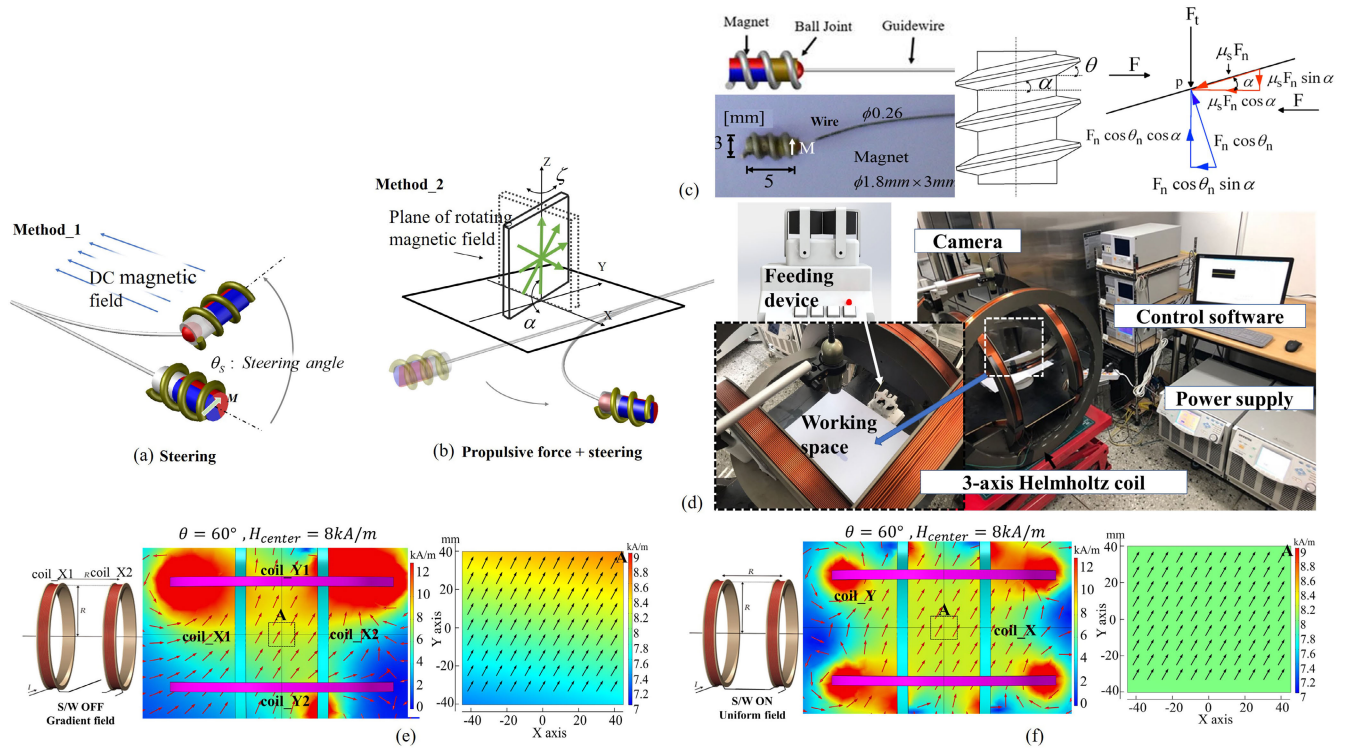


FIGURE 2. Steering methods according to type of magnetic field: (a) steering method using dc magnetic field (uniform or gradient fields), (b) method to control steering and active locomotion using a rotating magnetic field, (c) fabricated end-effector using the spiral mechanism, and (d) three-axis Helmholtz coil-based magnetic manipulation system. (e) Simulation results (gradient field distribution) to generate steering angle of 60° using coil_Y1 and coil_X1. (f) Simulation results of a uniform field distribution for steering angle of 60° using Helmholtz coils (X and Y axis [mm]).

where F_f is the friction force opposing the movement on the blade surface: $F_f = \mu_s F_n$; F_n is the reactive force, and $F_n = F_t / (\cos \beta_n \cos \delta - \mu_s \sin \delta)$; μ_s is the friction coefficient; and β_n and δ respectively represent the blade angle and lead angle. To enhance the steering and active locomotion of the robotic guidewire, we utilized a magnetic manipulation system based on a three-axis Helmholtz coil, as shown in Fig. 2 (d). The control system can generate both rotating magnetic fields and gradient and uniform dc magnetic fields to enable the control of the two steering angles. The strength of the magnetic field in the Helmholtz coil can be expressed as follows:

$$H_{0(x,y,z)} = \begin{pmatrix} \frac{NI_m R_x^2}{(R_x^2 + d^2)^{3/2}} & \frac{NI_m R_y^2}{(R_y^2 + d^2)^{3/2}} & \frac{NI_m R_z^2}{(R_z^2 + d^2)^{3/2}} \end{pmatrix} \quad (3)$$

where H_x , H_y , and H_z represent the strengths of the magnetic field in the three-axis coil system; R is the radius of the coil; and d is the distance between the coils for a Helmholtz coil. N denotes the number of turns, and I_m is the current amplitude in the coil. Two methods exist to control the coil, depending on the type of magnetic field applied when steering the guidewire. Let us assume, for example, that the guidewire is steering in the xz plane. When a dc magnetic field is used, the steering angle θ_s is determined by the ratio of the strengths

of the magnetic fields between H_x and H_z in the x-axis and z-axis coils: $\tan \theta_s = H_x / H_z$.

In the manufactured coil system, there are two coils aligned along each of the three axes, paired by a switch. When the switch is on, they are configured as a Helmholtz coil, which generates a uniform magnetic field; while the switch is off, they make a Maxwell coil, which generates a gradient field. Figure 2 (e) shows the simulation result of generating a steering angle of 60° using the gradient field. In this case, coil_X1 and coil_Y1 generate a gradient magnetic field that produces both a steering angle and a pulling force (translational force). Figure 2 (f) shows the simulation result of turning on the switch and constructing a Helmholtz coil to generate a steering angle of 60° . We can selectively use gradient and uniform magnetic fields by controlling the switch. Region A (8 cm x 8 cm) shows the gradient and uniform field distribution. Basic steering tests were performed in this area.

When rotating magnetic fields are produced by Helmholtz coil, the applied rotating magnetic torque generates rotation of the end-effector. In this case, the end-effector produces the thrust force for active locomotion.

To realize steering and locomotion using a rotating magnetic field, we can control the direction of plane of a rotating magnetic field using the control angles α and ζ (see Fig. 2 (b)), as mentioned previously. The initial

generation of the rotation magnetic field is the yz plane. Under the condition, the controlled magnetic field can be expressed as follows:

$$\begin{pmatrix} H_x \\ H_y \\ H_z \end{pmatrix} = H_{0(x,y,z)} \begin{pmatrix} \cos \zeta \sin \alpha \sin \omega t - \sin \zeta \cos \omega t \\ \cos \zeta \cos \omega t + \sin \zeta \sin \alpha \sin \omega t \\ \cos \alpha \sin \omega t \end{pmatrix} \quad (4)$$

where ω is the angular velocity of the current source; and α and ζ are the control angles for the plane of the rotating magnetic field. The guidewire is controlled in the three-axis Helmholtz coil system.

Table 1 lists the specifications of the fabricated coils. In the coil system, the strength of the applied magnetic field was up to 10 kA/m. The coil system could generate a uniform magnetic field within 12 cm of the center in each direction, as shown in Fig. 3 (a) when the switch was ON (closed) for each pair of coils (See Fig. 2 (f)). Although the design specifications of the three pairs of Helmholtz coils are different, they are designed to generate the same strengths of magnetic field for the same current (see Table 1 and Fig. 3). Figure 3 (b) shows the distributions of the gradient magnetic field at coil_X1, coil_Y1, and coil_Z1 when the switches were opened (OFF). The electromagnetic control system can configure the coils as either a Helmholtz or Maxwell coil by controlling the switch state. Therefore, in the Helmholtz coil state, steering and active locomotion can be achieved using a uniform dc or a rotating magnetic field, whereas Maxwell coils provide steering due to a gradient magnetic field. In this case, the force acts in the direction of increasing magnetic density. The control characteristics can change depending on the types of coils in the electromagnetic manipulation system.

TABLE 1. Specification of the designed coils.

	X-axis coil	Y-axis coil	Z-axis coil	Unit
Coil resistance	11.8	23.75	9.5	Ω
Inner diameter	512	664	416	mm
Outer diameter	600	760	480	mm
Number of turns	960	1200	760	

III. EXPERIMENTAL VERIFICATION AND RESULTS

To verify the proposed mechanism, two types of end-effectors were prepared one involving the ball joint and one without the ball joint. Using the two mechanisms, we compared the steering angles in the dc magnetic field and rotating magnetic field. In addition, we observed the performance of active locomotion with steering. For these experiments, we applied field strengths of 2, 4, 6, and 8 kA/m to the guidewire, and the driving frequency of the rotating magnetic field was less than 8 Hz. Steering and movement tests were performed in silicone oil and drilling tests were performed in agar jelly.

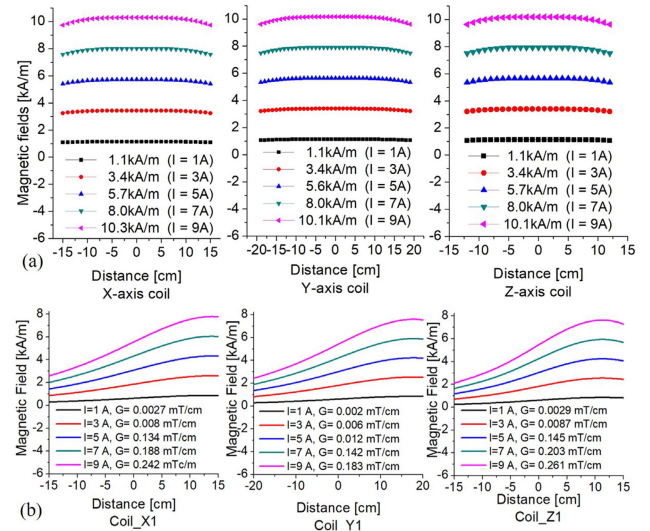


FIGURE 3. Magnetic field distributions in the coil system: (a) Results in Helmholtz coil (switch ON) and (b) the results of a single coil at three-axis (switch OFF).

A. ANALYSIS OF STEERING ABILITY

The proposed guidewire includes a spiral-type magnetic microrobot with a ball joint to realize steering and active locomotion. The fabricated ball joint can generate a joint angle of up to 45° , as shown in Fig. 4. Therefore, the developed guidewire has a minimum steering angle of 45° without the deformation of guidewire. The total steering angle is the sum of the joint angle and the wire angle, and the wire angle depends on the distance between the tip (microrobot) and the bending point at constant flexibility. We observed the total steering angles with the distance between the tip and the bending points being 1, 2, and 3 cm.

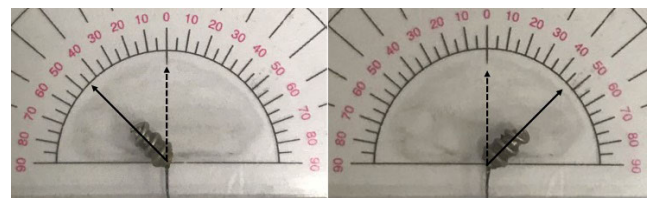


FIGURE 4. Observation of the maximum ball-joint angle of the proposed mechanism.

In narrow pathways such as blood vessels, it is necessary that the distance between the tip and the bending point is small for effective steering of the guidewire. Typically, the steering of magnetic guidewire is driven by the dc magnetic field (gradient field). However, because we used a spiral-type magnetic microrobot, we used two types of magnetic fields: a dc field (gradient field) and a uniform rotating magnetic field. The two magnetic fields corresponded to different steerabilities. The total steering angle is the sum of the joint angle and the wire angle, and the wire angle depends on the distance between the tip (microrobot) and the bending

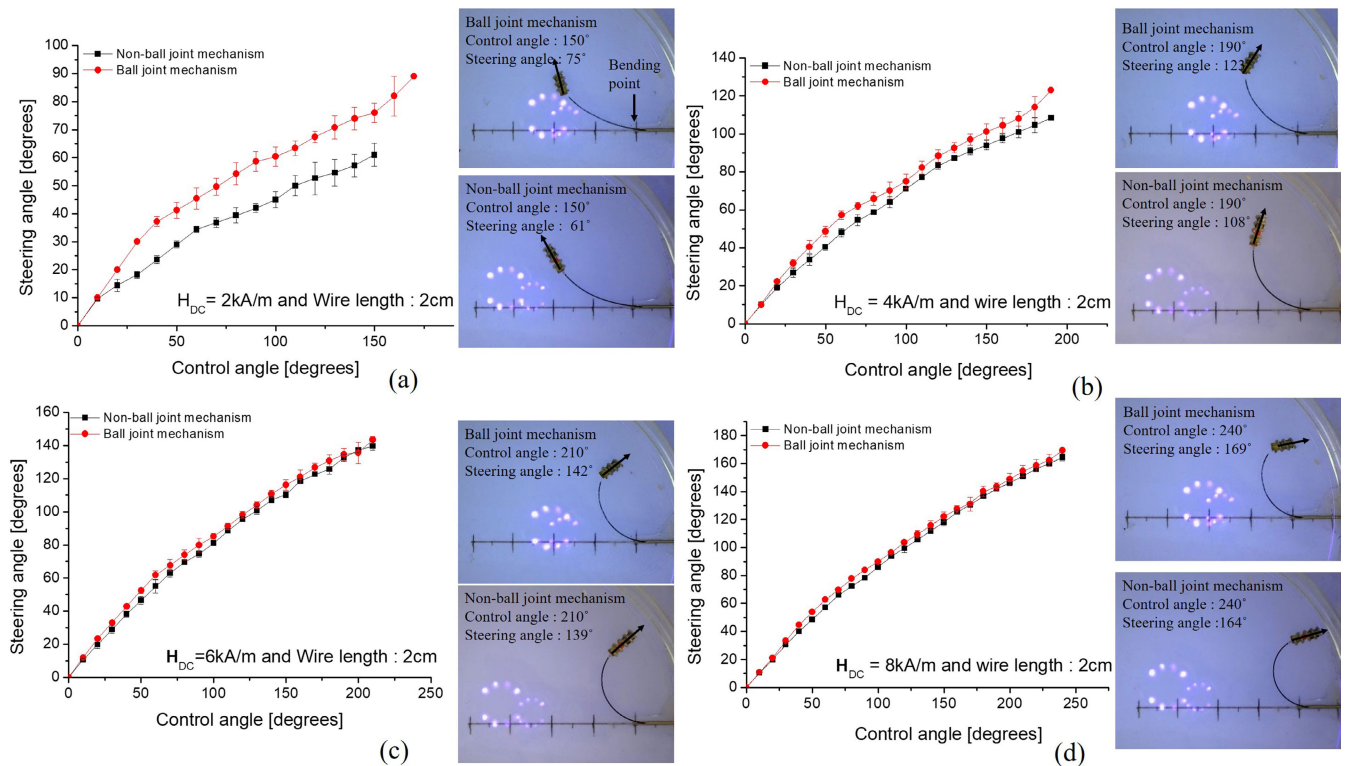


FIGURE 5. Comparison of steering angles of the ball-joint type and non-ball-joint type guidewire in dc magnetic field: the bending point is fixed at 2 cm from the end-effector. Results for steering angle for control angle of (a) up to 150° at field of 2 kA/m, (b) up to 200° at 4 kA/m, (c) up to 220° at 6 kA/m, and (d) up to 250° at 8 kA/m. The magnetic field strength determined the range of the control angles and steering angles.

point at constant flexibility. Figure 5 shows the variations of the steering angle according to changes in the control angles at the applied dc gradient field strengths of 2, 4, 6, and 8 kA/m with a distance of 2 cm between the tip and the bending point. The strengths of the four fields are always constant in the center of the working space. The applied dc fields are generated by coil_Y1 and coil_X1. Therefore, the control fields become dc gradient fields (see Fig. 2 (e)).

In the experiments, we could confirm the improvement of the steering angle by the ball-joint under a low strength magnetic field. Because of the elastic property of the wire, the rotation (steering) of the ball-joint was easier to realize than the bending of the wire. Figure 5 (a) shows the steering results of both the ball-joint mechanism and non-ball-joint mechanism at a magnetic field of 2 kA/m. When the control angle was 40°, the ball-joint mechanism generated a steering angle of 40°, whereas the non-ball-joint mechanism generated a steering angle of approximately 25°, depending on the wire property. When the control angle was 150°, the two mechanisms generated steering angles of up to 75° and 61°, respectively. At a strength of 4 kA/m, the difference between the two steering angles decreased due to the increased magnetic torque, which increased the wire angle (bending). At the strength of 4 kA/m, the maximum steering angles for the ball-joint and non-ball-joint mechanisms were respectively 123° and 108°, as shown in Fig. 5 (b). When the applied magnetic field strengths were 6 and 8 kA/m, the steering angles

for the ball-joint and non-ball-joint mechanisms were nearly similar, as shown in Figs. 5 (c) and (d) because the steering angle in the gradient field is affected by the pulling force (magnetic force) as well as the magnetic torque. Therefore, the greater the intensity of the applied dc field, the smaller the difference between the two steering angles (ball-joint and non-ball-joint mechanisms).

Figure 6 shows the steering angles for both the ball-joint and non-ball-joint mechanisms, corresponding to changes in the control angles in rotating magnetic fields. The applied field strengths were 2, 4, 6 and 8 kA/m at a constant frequency of 1 Hz. For steering, the plane of the rotating magnetic field was changed from the YZ plane to the ZX plane by controlling the angle α (see Fig.2 (b)). The applied rotating magnetic field produced relatively lower steering angles than those generated by the dc magnetic field. Furthermore, in the case of the rotating magnetic field, the steering angles corresponding to the ball-joint and non-ball-joint mechanisms exhibited a considerable difference.

The applied field with a strength of 2 kA/m exhibited the largest difference in the steering angles for the ball-joint and non-ball-joint mechanisms. When the maximum control angle was 120°, the difference in the steering angles was 51°, as shown in Fig. 6 (a).

From the applied field of 4 kA/m, the control angles were limited to 130° for both mechanisms. In the case of the ball-joint type, the increase rate of the steering angle

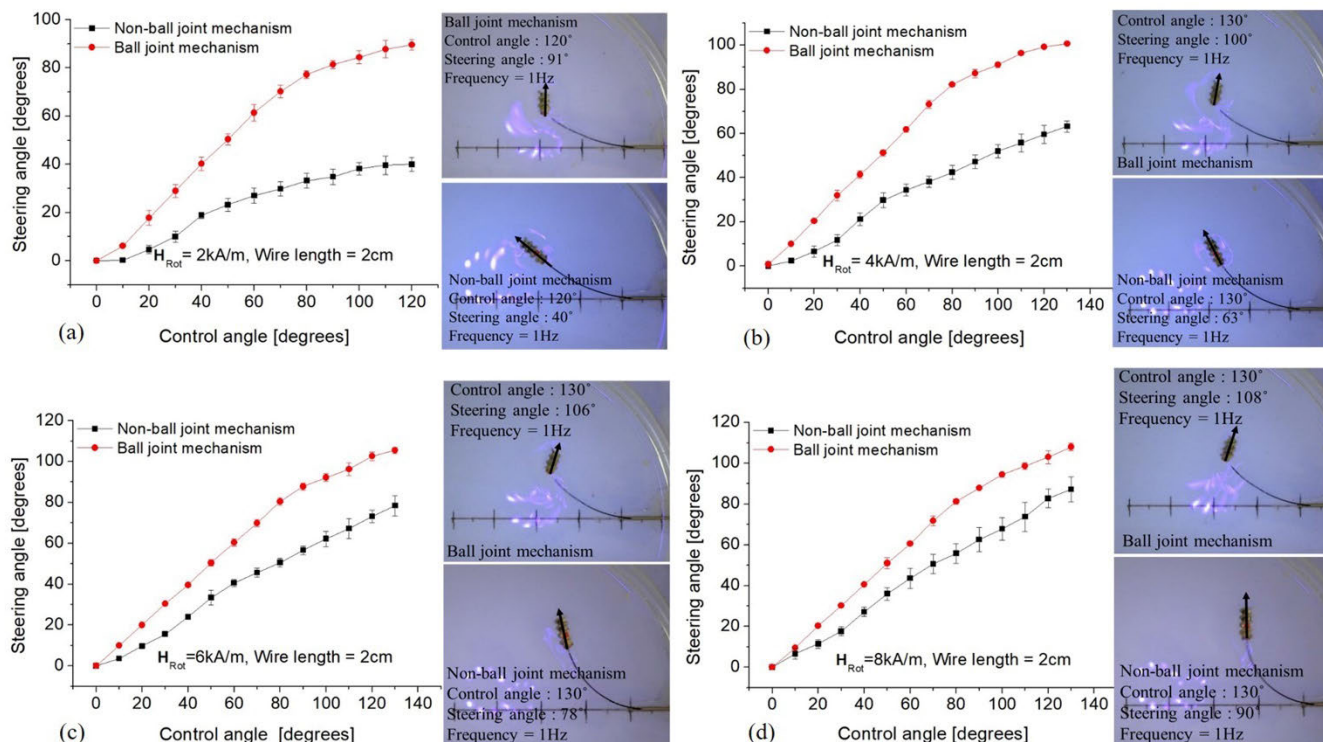


FIGURE 6. Comparison of steering angles for ball-joint and non-ball-joint type guidewires in rotating magnetic field: Results for steering angle at (a) 2 kA/m, (b) 4 kA/m, (c) 6 kA/m, and (d) 8 kA/m.

decreased for control angles higher than 80° because of the elastic property of the wire. Under the applied fields with a strength of 4, 6, and 8 kA/m, the ball-joint type generated the maximum steering angles of 100°, 106°, and 108°, respectively, whereas the non-ball-joint type mechanism generated steering angles of 63°, 78°, and 90°, respectively, as shown in Fig. 6 (b)–(d). A uniform rotating magnetic field provides magnetic torque for steering without the pulling force. Therefore, the difference between the two steering angles is relatively larger when using our mechanism, compared to the gradient field. Further, we analyzed the steering characteristics according to the applied field types and joint mechanisms.

The results presented in Figs. 5 and 6 indicate that the ball-joint mechanism demonstrated excellent steering characteristics, especially at low magnetic field strengths. The maximum control angle and steering angle values for the ball-joint mechanism under dc and rotating magnetic fields, according to the bending points (1, 2, and 3 cm) of the wire, are summarized in Table 2. The maximum control angle varies, as the rotating magnetic field uses a uniform rotating magnetic field and the dc field uses a gradient magnetic field. Each type of field produces different maximum steering angle. The maximum control angle also depends on the strength of the field and the length of the wire. It can be noted that when the bending point was 1 cm, under a rotating magnetic field of 8 kA/m, the maximum control angle and steering angle values were 100° and 74°, respectively. At the

TABLE 2. Comparison of maximum control and steering angle.

H [kA/m]	Bending points	Bending points					
		1cm		2cm		3cm	
		θ_c	θ_s	θ_c	θ_s	θ_c	θ_s
2	Rot	100	74	120	91	140	100
	DC	160	75	150	76	140	78
4	Rot	100	72	130	101	150	115
	DC	170	93	190	123	160	116
6	Rot	100	73	130	105	160	127
	DC	200	116	210	144	240	173
8	Rot	100	74	130	108	160	135
	DC	230	136	240	169	250	189

same bending point, the dc field of 8 kA/m generated a control angle (θ_c) of 230° and steering angle (θ_s) of 136°.

A shorter distance between the bending point and end-effector of the guidewire corresponded to a larger force required for steering. Figure 7 shows the COMSOL simulation results of the relationship between the steering angle and bending stress at bending points of 1, 2, and 3 cm. To obtain the simulation results, we experimentally measured the steering angle and bending displacement of the wire. The measured values were applied to the simulation to obtain Fig. 7. A nylon wire with density, Young’s modulus, and Poisson’s ratio of 1150 kg/m³, 2 × 10⁹ Pa, and 0.4, respectively, was used. In a certain joint angle range, no wire angle is generated

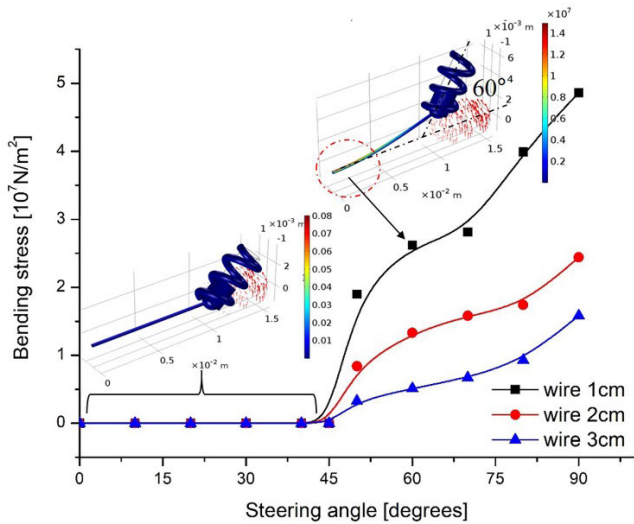


FIGURE 7. Simulation results: Relationship between bending stress and steering angle for different bending points. The bending stress is zero up to a certain ball-joint angle.

and the bending stress is zero. Bending stress is generated when the steering angle exceeds the ball-joint angle. For a steering angle of 60°, the bending points of 1, 2, and 3 cm corresponded to a generated bending stress of 2.6, 1.4, and $0.5 \times 10^7 \text{N/m}^2$, respectively. Therefore, a smaller bending

point corresponds to a larger force or torque required to steer.

B. ANALYSIS OF STEERING ABILITY AND MOBILITY

If we consider only the steering angle, the dc magnetic field leads to more desirable results than the rotating magnetic field does for the proposed mechanism. However, the end-effector is a spiral-type magnetic microrobot. Therefore, we consider the improvement of steering with stable locomotion. Figure 8 shows the movement with steering using the proposed mechanism in the dc and rotating magnetic fields. The experiments were conducted using a vision-based feedback system. Therefore, entering the destination coordinates into the control system automatically controlled the magnitude and phase of the current, so the guidewire reached the destination. In addition, the speed of the feeding device and the rotational speed of the robot could be set to be synchronized or asynchronous.

The aim of the experiments was to achieve a steering angle of 120° and have the guidewire, which was propelled by a feeding device at a constant velocity of $1.87 \times 10^{-3} \text{m/s}$, reach a given destination.

To analyze the stability of movement, we observed the moving trajectory by using a video camera with an image processing technique. Figure 8 (a) shows the driving current profile (the ratio between coil Y2 and X1) and the movement with steering from coil Y2 and X1 in the dc field.

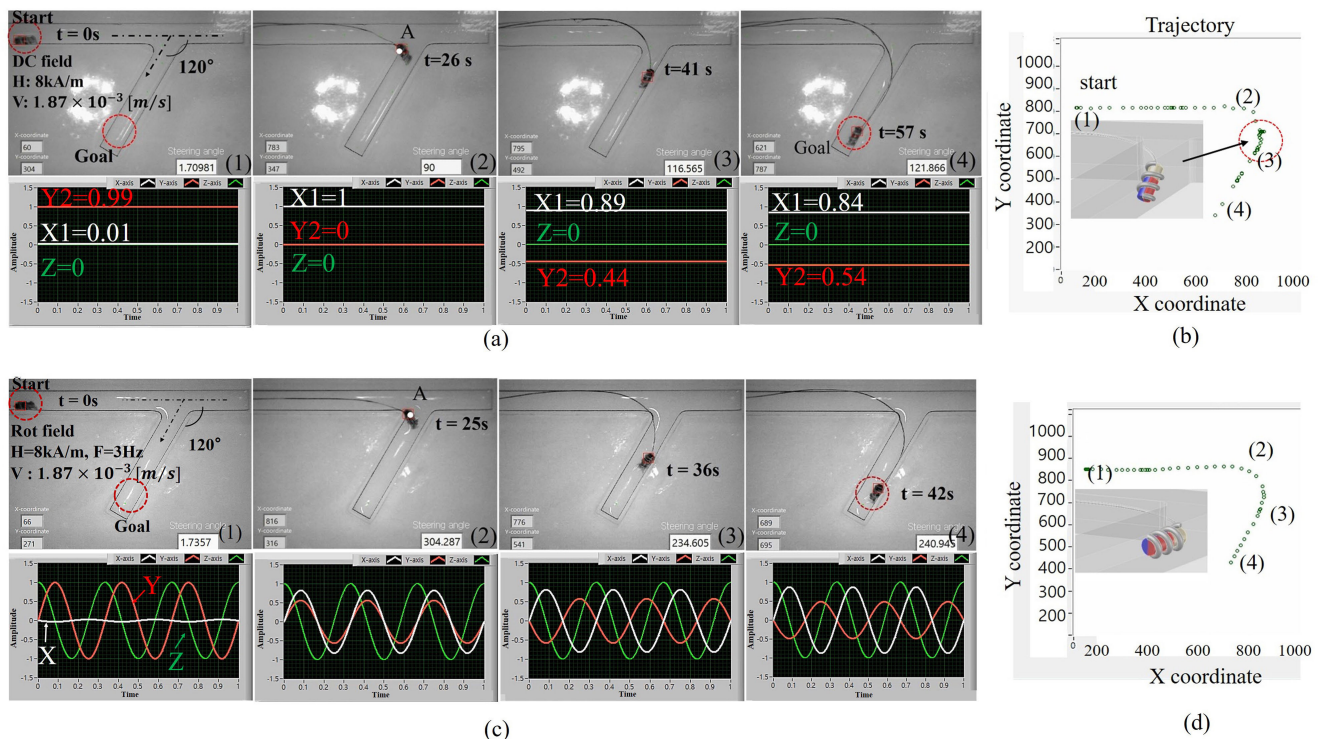


FIGURE 8. Movement with steering of developed guidewire using a feeding device in (a) dc magnetic field with current profiles, (b) trajectory of the guidewire using the gradient field, (c) rotating magnetic field with current profiles. Rot denotes the rotating magnetic field; H is the strength magnetic field; and V is the feeding velocity, and (d) trajectory of the guidewire using the rotating magnetic field.

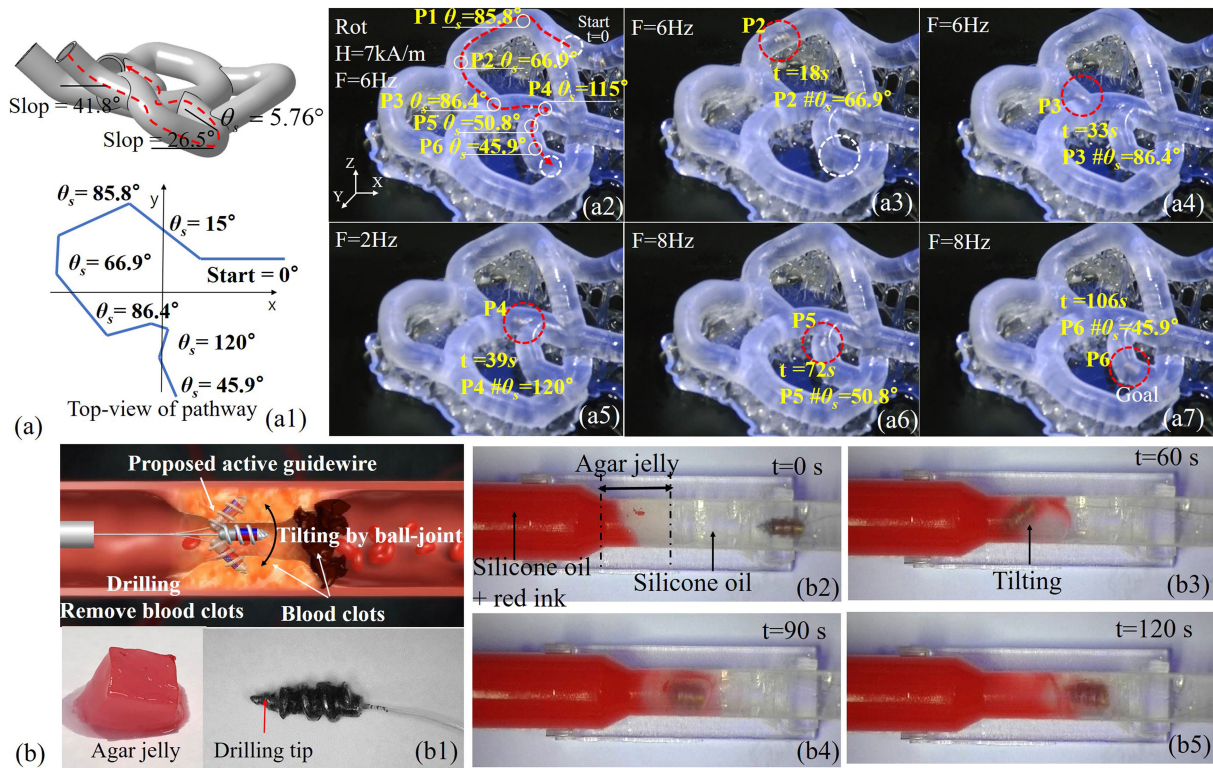


FIGURE 9. (a) Experiment for active locomotion and steering without the feeding device: (a1) Design of three-dimensional blood vessel phantom and moving path with the desired steering angles: inner diameter of pathway is 6 mm; (a2 to a7) movement in the phantom model: Silicone oil with a viscosity of 3000 cst was used in the phantom model. (b) Experiment for drilling function: (b1) Concept of drilling function to remove blood clots; the prepared agar jelly includes agar powder of 0.32 wt%. (b2 to b5) experimental setup and actuation for drilling with active locomotion without the feeding device.

The applied dc field was fixed at 8 kA/m at the center of working space. In addition, the experiment did not use the Z-axis coil because steering was performed in the XY plane. The guidewire took 57 s to reach the destination, and 15 s to reach from points 2 to point 3. The moving direction and head direction must be aligned to ensure stable movement. However, it was confirmed that the trajectory, measured using position tracking with a video camera, from point 2 to point 3 was unstable because the head direction was not aligned to the moving direction due to the influence of the joint mechanism, as shown in Fig. 8 (b). Figure 8 (c) shows the movement and steering in the uniform rotating magnetic field generated by three pairs of Helmholtz coils, in each axial direction.

In this case, the feeding device propelled the guidewire, and the robot was rotated under a rotating field with a strength and frequency of 8 kA/m and 2 Hz, respectively. X, Y, and Z denote the profile of the current delivered to each coil for active locomotion with steering. The guidewire was steered in a straight line along the X axis from the start point to point A. For this type of movement, the rotating magnetic field was in the YZ plane. Therefore, current was applied to the Y and Z-axis coils with a phase difference of 90°. To steer to point A, the YZ plane of a rotating magnetic field was rotated to the ZX plane by the steering control angle ζ (see Fig. 2 (b)). Therefore, the current in the X-axis coil was activated.

In the rotating magnetic field, the direction of the head (robot) was not inclined by the ball-joint because the robot rotated around the rotation axis. Therefore, when the guidewire was moved in the rotating magnetic field, the guidewire exhibited stable movement, as can be confirmed by the moving trajectory. We performed both experiments 10 times each. Under the dc magnetic field, an unstable trajectory was observed six times, whereas when the rotating magnetic field was used, a stable trajectory was obtained in each run, as shown in Fig. 8 (d). Figure 9 shows the experimental results of the active locomotion and drilling function in the rotating magnetic field without the feeding device. The experiments were controlled manually, using a joystick. Because the experimental apparatus allows for three-dimensional movement, the guidewire is moved along a path by controlling the angles α and ζ in Eq. (4) (see Fig. 2 (b)). Because of the right-handed screw mechanism being applied on the body, the robot produced active locomotion via rotation of the body. The clockwise rotating magnetic field generated a forward movement, whereas the counterclockwise rotating field generated a backward movement. We fabricated a three-dimensional blood vessel phantom model using 3D printing. Figure 9 (a1) shows the moving path and the desired steering angle. In the phantom model, the maximum steering angle was 120°. The strength

of rotating magnetic field was fixed at 7 kA/m, and the driving frequency was varied from 2 Hz to 8 Hz. The guidewire took 106 s to reach the destination using only the propulsive force of the robot. To move from P1 to P5, it was necessary to steer by 120°. In this case, it took 31 s to move and steer under a rotation of 2 Hz. In the case of the guidewire having a steering angle of 90° or less, the success rate was 90% or more regardless of the driving frequency. However, for a steering angle of 120°, from P4 to P5, the success rate under 5 Hz was 60% or more, whereas that under 8 Hz was less than 50%. The rotating field of 2 Hz thus demonstrated a success rate of 80%. The developed active guidewire was noted to be able to successfully realize the drilling function to remove blood clots.

Figure 9 (b1) shows the concept of drilling to remove clots in the blood vessel, along with the fabricated soft agar jelly and the added drill tip at the robot. Because of the ball-joint at the guidewire, the robot can generate a tilting motion, which, along with the rotation of the robot can effectively remove blood clots. To verify the drilling function, we incorporated silicone oil with a viscosity of 3000 cst along with red ink, and agar jelly with a thickness of 1 cm, as shown in Fig. 9 (b2). Experiments were performed to remove the agar jelly while generating forward movement, backward movement, and a tilting motion while varying the frequency up to 8 Hz at fixed field of 5kA/m. The rotating magnetic field was in the YZ plane and the control angle α was adjusted up to 50° for the tilting motion. It was confirmed that the red colored oil was displaced to the right after 60 s. So far, several research groups have performed investigations on magnetic field-induced microcatheters and guidewires. However, in most studies, the magnetic field was relatively strong, and a steering angle of 90° or less was generated. In contrast, the developed mechanism using a spiral microrobot and ball-joint can be steered in an extremely low intensity field (2.5 mT). The mechanism can move actively, precision control is possible, and the degree of freedom is improved by the ball-joint. Typically, because the length of the guidewire is 1.5 m, the spiral microrobot head cannot tow the guidewire completely. For actual clinical application, a feeding device to push the guidewire is required. However, the spiral microrobot can realize towing for distances less than 30 cm. Under the 30 cm movement, the end-effector can provide precision motion control. By conducting performance evaluation in various environments, it was confirmed that the steering angle was improved by the ball joint, which is especially advantageous in low magnetic fields. Using the microrobot as a guidewire, the performance in realizing various aspects including precision steering control, stable movement, and drilling function was satisfactory. Therefore, the developed guidewire can apply to both diagnostic tool and therapy.

The developed robotic guidewire does not generate heat during movement and is not affected by the earth magnetic field. In general, implantable devices have to be considered for toxicity. However, the issue of toxicity analysis

was ignored because the guide wire is temporarily used and removed from the body.

IV. CONCLUSION

To improve the steering angle of active guidewire in low magnetic fields of up to 8 kA/m (10 mT), we proposed a novel guidewire mechanism. A guidewire and a control system using a microrobot that can generate propulsive force and a ball joint mechanism that can improve the steering angle in a rotating magnetic field was developed. Owing to the ball-joint, a steering angle of 75° could be generated under a magnetic field strength of 2 kA/m (intensity: 2.5 mT).

It is possible to realize precise movement and steering by controlling the rotating direction and changing the rotation axis of the rotating magnetic field. In addition, the robot mechanism can perform drilling function for removing thrombi during movement, and tilting can be performed by the ball-joint, thereby improving the drilling effect. To verify these functions, we conducted simulations and various experiments. However, the conducted tests were basic tests to verify the mechanism. To develop an actual system, considerable research pertaining to the testing, toxicity testing, and animal experiments performed using the proposed mechanism with commercially available guidewires must be performed.

REFERENCES

- [1] L. Zhang, J. J. Abbott, L. Dong, B. E. Kratochvil, D. Bell, and B. J. Nelson, "Artificial bacterial flagella: Fabrication and magnetic control," *Appl. Phys. Lett.*, vol. 94, no. 6, Feb. 2009, Art. no. 064107.
- [2] J. J. Abbott, K. E. Peyer, M. C. Lagomarsino, L. Zhang, L. X. Dong, I. K. Kaliakatsos, and B. J. Nelson, "How should microrobots swim?" *Int. J. Robot. Res.*, vol. 28, nos. 11–12, pp. 1434–1447, Nov. 2009.
- [3] A. Ghosh and P. Fischer, "Controlled propulsion of artificial magnetic nanostructured propellers," *Nano Lett.*, vol. 9, no. 6, pp. 2243–2245, Jun. 2009.
- [4] B. J. Nelson, I. K. Kaliakatsos, and J. J. Abbott, "Microrobots for minimally invasive medicine," *Annu. Rev. Biomed. Eng.*, vol. 12, no. 1, pp. 55–85, Jul. 2010.
- [5] H. Choi, K. Cha, S. Jeong, J.-O. Park, and S. Park, "3-D locomotive and drilling microrobot using novel stationary EMA system," *IEEE/ASME Trans. Mechatronics*, vol. 18, no. 3, pp. 1221–1225, Jun. 2013.
- [6] S. H. Kim and K. Ishiyama, "Magnetic robot and manipulation for active-locomotion with targeted drug release," *IEEE/ASME Trans. Mechatronics*, vol. 19, no. 5, pp. 1651–1659, Oct. 2014.
- [7] S. Pané, O. Egeneman, K. M. Sivaraman, T. Lühmann, H. Hall, and B. J. Nelson, "Strategies for drug-delivery and chemical sensing using biomedical microrobots," in *Proc. IEEE Int. Conf. Nano/Mol. Med. Eng.*, Dec. 2010, pp. 148–152.
- [8] S. Yim and M. Sitti, "Shape-programmable soft capsule robots for semi-implantable drug delivery," *IEEE Trans. Robot.*, vol. 28, no. 5, pp. 1198–1202, Oct. 2012.
- [9] A. K. Hoshiar, T.-A. Le, F. U. Amin, M. O. Kim, and J. Yoon, "Studies of aggregated nanoparticles steering during magnetic-guided drug delivery in the blood vessels," *J. Magn. Magn. Mater.*, vol. 427, no. 1, pp. 181–187, Apr. 2017.
- [10] H. M. Ko and S. H. Kim, "Preliminary validation of robotic control of magnetic particles for targeted hyperthermia," *J. Magn.*, vol. 23, no. 1, pp. 117–124, Mar. 2018.
- [11] J. Nam, W. Lee, J. Kim, and G. Jang, "Magnetic helical robot for targeted drug-delivery in tubular environments," *IEEE/ASME Trans. Mechatronics*, vol. 22, no. 6, pp. 2461–2468, Dec. 2017.
- [12] Y. Haga, T. Mineta, K. Totsu, W. Makishi, and M. Esashi, "Development of active catheter, active guide wire and micro sensor systems," *Interventional Neuroradiol.*, vol. 22, no. 7, pp. 125–130, 2002.

- [13] Y. Fu, H. Liu, W. Huang, S. Wang, and Z. Liang, "Steerable catheters in minimally invasive vascular surgery," *Int. J. Med. Robot. Comput. Assist. Surg.*, vol. 5, no. 4, pp. 381–391, Dec. 2009.
- [14] F. Ganet, M. Q. Le, J. F. Capsal, P. Lermusiaux, L. Petit, A. Millon, and P. J. Cottinet, "Development of a smart guide wire using an electrostrictive polymer: Option for steerable orientation and force feedback," *Sci. Rep.*, vol. 23, no. 1, 2015, Art. no. 15893.
- [15] F. Settecase, M. S. Sussman, M. W. Wilson, S. Hetts, R. L. Arenson, V. Malba, A. F. Bernhardt, W. Kucharczyk, and T. P. L. Roberts, "Magnetically-assisted remote control (MARC) steering of endovascular catheters for interventional MRI: A model for deflection and design implications," *Med. Phys.*, vol. 34, no. 8, pp. 3135–3142, Jul. 2007.
- [16] C.-H. Yu and S. H. Kim, "Multifunctional robotic guidewire system using spiral-type magnetic microrobot with magnetic manipulation," *J. Magn.*, vol. 21, no. 4, pp. 616–621, Dec. 2016.
- [17] T. Fukushi, S. Hoon Kim, S. Hashi, and K. Ishiyama, "Preliminary validation of Sm–Fe–N magnetic silicone rubber for a flexible magnetic actuator," *Smart Mater. Struct.*, vol. 23, no. 6, Jun. 2014, Art. no. 067001.
- [18] S. H. Kim, "3D helmholtz coil-based hybrid manipulation for active locomotion of magnetic micro/nano robot," *J. Magn.*, vol. 23, no. 4, pp. 578–583, 2018.
- [19] J. Li, X. Li, T. Luo, R. Wang, C. Liu, S. Chen, D. Li, J. Yue, S. Cheng, and D. Sun, "Development of a magnetic microrobot for carrying and delivering targeted cell," *Sci. Robot.*, vol. 3, no. 19, 2018, Art. no. eaat8829.
- [20] T. Xu, J. Yu, X. Yan, H. Choi, and L. Zhang, "Magnetic actuation based motion control for microrobots: An overview," *Micromachines*, vol. 6, no. 9, pp. 1346–1364, Sep. 2015.
- [21] F. Qiu and B. J. Nelson, "Magnetic helical micro- and nanorobots: Toward their biomedical applications," *Engineering*, vol. 1, no. 1, pp. 21–26, 2015.
- [22] B. J. Jang, J. K. Nam, W. S. Lee, and G. H. Jang, "A crawling magnetic robot actuated and steered via oscillatory rotating external magnetic fields in tubular environments," *IEEE/ASME Trans. Mechatronics*, vol. 22, no. 3, pp. 1465–1472, Mar. 2017.
- [23] S. M. Jeon, J. K. Nam, W. S. Lee, and G. H. Jang, "Selective navigating and unclogging motions of an intravascular helical magnetic millirobot actuated by external biaxial rotating magnetic field," *IEEE/ASME Trans. Mechatronics*, vol. 22, no. 3, pp. 1456–1464, Mar. 2017.
- [24] T. Krings, J. Finney, P. Niggemann, P. Reinacher, N. Lück, A. Drexler, J. Lovell, A. Meyer, R. Sehra, P. Schauerte, M. Reinges, F. J. Hans, and A. Thron, "Magnetic versus manual guidewire manipulation in neuroradiology: *In vitro* results," *Neuroradiology*, vol. 48, no. 6, pp. 394–401, Jun. 2006.
- [25] H. C. Clogenson, J. Dankelman, and J. J. van den Dobbelen, "Steerable guidewire for magnetic resonance guided endovascular interventions," *J. Med. Devices*, vol. 8, no. 2, 2014, Art. no. 021002.
- [26] S. M. Jeon and G. H. Jang, "Precise steering and unclogging motions of a catheter with a rotary magnetic drill tip actuated by a magnetic navigation system," *IEEE Trans. Magn.*, vol. 48, no. 11, pp. 4062–4065, Nov. 2012.
- [27] S. Jeon, A. K. Hoshiar, S. Kim, S. Lee, E. Kim, S. Lee, K. Kim, J. Lee, J. Kim, and H. Choi, "Improving guidewire-mediated steerability of a magnetically actuated flexible microrobot," *Micro Nano Syst. Lett.*, vol. 6, no. 1, p. 15, 2018.
- [28] S. Jeon, A. K. Hoshiar, K. Kim, S. Lee, E. Kim, S. Lee, J.-Y. Kim, B. J. Nelson, H.-J. Cha, B.-J. Yi, and H. Choi, "A magnetically controlled soft microrobot steering a guidewire in a three-dimensional phantom vascular network," *Soft Robot.*, vol. 6, no. 1, pp. 54–68, Feb. 2019.
- [29] N. Kim, S. Lee, W. Lee, and G. Jang, "Development of a magnetic catheter with rotating multi-magnets to achieve unclogging motions with enhanced steering capability," *AIP Adv.*, vol. 8, no. 5, May 2018, Art. no. 056708.



GUK-HONG JEON received the B.S. and M.S. degrees in electronics convergence engineering, Wonkwang University, Iksan, South Korea, in 2017 and 2019, respectively. He is currently an Engineer with CAMTIC Advanced Mechatronics Technology Institute for Commercialization, Jeonju, South Korea. His research interests include the design and control of magnetic micro-robot system.



SUNG HOON KIM (Member, IEEE) received the B.S. degree in electronic engineering from Yeungnam University, Gyeongsan, South Korea, in 2005, the M.S. degree in medical and biological engineering from Kyungpook National University, Daegu, South Korea, in 2007, and the Ph.D. degree in electrical communication engineering from Tohoku University, Sendai, Japan, in 2012. He is currently an Associate Professor with the Department of Electronics Convergence

Engineering, Wonkwang University, Iksan, South Korea. His research interests include magnetic sensors and actuators, multiscale magnetic micro/nano systems, magnetic hyperthermia, and implantable medical devices.

• • •